Analyst

ROYAL SOCIETY OF CHEMISTRY

PAPER

View Article Online
View Journal | View Issue

Cite this: *Analyst*, 2025, **150**, 3208

An indolizine-derived chemodosimeter with enhanced emission in a micellar environment for ppb-level detection of mercury ions†

Amanda Ana Pinheiro,‡ Ankit Thakuri,‡ Soumik Saha, Mainak Banerjee * and Amrita Chatterjee *

Received 6th May 2025,
Accepted 4th June 2025

DOI: 10.1039/d5an00502g

rsc.li/analyst

Mercury is a harmful heavy metal that gravely threatens the environment and organisms. In the current study, 2-(1,3-oxathiolan-2-yl)-1,3-diphenylindolizine (**DPIC-OS**) and 2-(1,3-dithiolan-2-yl)-1,3-diphenylindolizine (**DPIC-SS**) probes are designed by protecting a 1,3-diphenylindolizine-2-carbaldehyde (**DPIC-CHO**) with mercury-recognizable 1,3-dithiolane and 1,3-oxathiolane moieties and utilized for the selective detection of Hg^{2+} ions in a micellar medium. Hydrophobic probes **DPIC-OS** and **DPIC-SS** exhibit intense fluorescence in the confined environment of a micellar solution. A significant enhancement in fluorescence intensity was seen for these probes upon switching from organic to aqueous micellar media. Upon the incremental addition of Hg^{2+} ions, the probes display a fluorescence shift, exhibiting a bluish-green emission at 505 nm through the release of fluorescent **DPIC-CHO** in the working solution by the spontaneous cleavage of the thioacetal linkage. **DPIC-OS** was more efficient than **DPIC-SS**, and subsequent analytical studies were conducted with this probe. The **DPIC-OS** exhibited no or insignificant response towards numerous common anions, cations, and small molecules, affirming its selectivity to Hg^{2+} ions and offering a low limit of detection (LOD) of 3.2 ppb (16.2 nM). The real-sample analysis by spiking mercury ions in water showed excellent percentage recoveries.

1. Introduction

The presence of toxic metal ions like mercury, lead, cadmium, chromium, and arsenic in the environment is a major source of various human health disorders.[1] Of these, mercury is notably one of the most toxic heavy metals that are abundantly distributed in air, soil, and water.[2,3] Mercury emissions are primarily associated with anthropogenic activities, such as oil refining, coal and gold mining, and chemical manufacturing, which together cause severe ecological damage.[4–6] Once released into the environment, mercury undergoes chemical transformations that enhance its bioaccumulation in aquatic ecosystems, especially in fish and seafood, thereby increasing the intake by humans through dietary consumption.[7–9] Human exposure to mercury through contaminated food or industrial activities results in severe health complications like neurological disorders, renal failure, cardiovascular disease, impaired cognitive and motor functions, *etc.*[10–13] These issues are specifically prevalent in highly populated countries such as India, where water-based food items form an integral part of dietary practices.[14] Indian aquatic systems, including coastal waters, have shown significant mercury contamination according to environmental studies, as elevated levels of mercury are present in sediments and suspended particulates.[15–17] Due to the severe toxicity associated with mercury, regulatory agencies such as the U.S. Environmental Protection Agency (USEPA) have implemented a maximum allowable mercury concentration of 2 ppb in drinking water, whereas, the World Health Organization (WHO) permits up to 50 ppb in agricultural soils, which underscores the urgent need for advanced analytical methods capable of detecting mercury ions with high sensitivity and selectivity.[18,19] Over the years, significant progress has been made in the development of analytical techniques for mercury detection, ranging from conventional methods to emerging technologies, such as atomic absorption spectroscopy (AAS),[20] cold vapor atomic fluorescence spectrometry,[21] inductively coupled plasma mass spectrometry (ICP-MS),[22] electrochemical methods,[23] and anodic stripping voltammetry (ASV).[24] While these methods offer high precision

Department of Chemistry, Birla Institute of Technology and Science Pilani, KK Birla Goa Campus, Goa 403726, India. E-mail: mainak@goa.bits-pilani.ac.in, amrita@goa.bits-pilani.ac.in; Fax: +91-832-255-7031; Tel: +91-832-2580-347, +91-832-2580-320

†Electronic supplementary information (ESI) available: Experimental details, absorption and emission spectra, tables of comparative studies, and NMR data. See DOI: https://doi.org/10.1039/d5an00502g

‡These authors contributed equally.

and quantitative detection capabilities, they are often associated with significant limitations like expensive instrumentation, skilled operators, and extensive sample pretreatment, which collectively restrict their accessibility and practical applications in routine monitoring scenarios.

Colorimetric and fluorometric methods have gained widespread recognition for their simplicity, selectivity, and high sensitivity, making them invaluable tools across diverse fields such as environmental monitoring, analytical chemistry, biology, and medicine.[25,26] Recent advancements have leveraged both Hg-ligand complexes and Hg-induced irreversible chemical reactions to detect Hg^{2+} in biological and environmental systems.[27,28] Among these, chelation-based fluorescent probes have proven particularly effective, often employing an on–off fluorescence mechanism in which Hg^{2+} quenches fluorescence by enhancing spin–orbit coupling upon analyte binding.[29,30] The strong thiophilic affinity of Hg^{2+} has facilitated the development of chemodosimeters incorporating thiourea,[31] thiones,[28] benzothiazole,[32] and thioacetal receptors,[33–37] yielding high sensitivity and robust signal-to-noise ratios for Hg^{2+} detection. However, a notable limitation of these small hydrophobic chemosensors is the requirement of some amount of organic solvent in aqueous–organic mixtures during spectroscopic analysis, which greatly compromises the biocompatibility of these sensing systems and often leads to reduced fluorescence intensity.[38–40] Furthermore, as mercury detection is primarily performed in aqueous media, the use of organic solvents proves detrimental to the detection sensitivity of these probes.[41,42] A probable solution to the insolubility of hydrophobic chemosensors lies in nature, which uses only aqueous media for any chemical transformations or biological functions. The use of amphiphilic surfactants in water not only forms micellar non-entities to encapsulate hydrophobic fluorophores[43–45] but also enhances their fluorescence intensity within the nanoconfined space in a synergistic manner.[46] By continuing our recent work on mercury detection in aqueous systems,[47,48] we focused on developing an indolizine-based chemodosimeter for selective and sensitive detection of mercury ions. The indolizine scaffold offers considerable advantages due to its synthetic versatility, enabling photophysical tunability and large Stokes shifts, which are crucial for chemosensing applications.[49,50] To this end, we designed **DPIC-OS** and **DPIC-SS** to specifically target Hg^{2+} ions with high efficiency and selectivity, exploiting the high thiophilic affinity of mercury. The nonpolar hydrophilic nature of **DPIC-OS** and **DPIC-SS** limits their solubility in aqueous media, restricting their effectiveness for mercury detection in water. However, a surfactant CTAB-derived microenvironment could overcome this difficulty for these probes.

2. Results and discussion

2.1 Design and synthesis

In our endeavor to develop a chemosensor for mercury ions from a barely explored fluorescent indolizine scaffold, we envisaged utilizing the thiophilic nature of mercury. Towards this objective, two probes, **DPIC-OS** and **DPIC-SS**, were synthesized *via* a two-step process. Firstly, **DPIC-CHO** was prepared from the cycloaddition of cinnamaldehyde and 2-benzoylpyridine using a well-reported procedure (Scheme S1, ESI†).[51] Following that, **DPIC-CHO** was treated with 2-mercaptoethan-1-ol and ethane-1,2-dithiol separately in the presence of $BF_3{\cdot}OEt_2$, in a typical protection reaction, to obtain **DPIC-OS** and **DPIC-SS**, respectively (Scheme 1 and Scheme S2, ESI†). The formation of the probes was characterized by NMR and mass spectrometry. The presence of a peak at δ 10.01 ppm in the ^{1}H NMR spectrum and a peak at δ 188.0 ppm in the ^{13}C NMR spectrum confirms the formation of **DPIC-CHO**. For **DPIC-OS** and **DPIC-SS**, the omission of the signature peaks of the –CHO group indicated the formation of thioacetyl products (**DPIC-OS** and **DPIC-SS**). Additionally, the presence of new peaks at δ 2.5–3.0 ppm in the ^{1}H NMR spectrum and at δ 35–50 ppm in the ^{13}C NMR spectrum further confirms the incorporation of the dithiol and mercaptoethanol moieties. The mass spectra of **DPIC-OS** and **DPIC-SS** exhibited expected peaks at *m*/*z* 358 and 374 corresponding to their $[M + H]^+$, explicitly confirming the formation of the desired probes.

2.2 Photophysical properties and optimization of the sensing assembly

To establish a sensing system for mercury ions, the photophysical properties of three compounds, **DPIC-CHO**, **DPIC-OS**, and **DPIC-SS**, were evaluated *via* UV-Vis and fluorescence spectroscopy. In UV-Vis studies, **DPIC-CHO** exhibited a prominent absorption band at 400 nm, while **DPIC-OS** and **DPIC-SS** exhibited absorption bands at 290 nm with a shoulder at 380 nm in organic solvents (Fig. S1a–c, ESI†). Upon excitation at 400 nm, **DPIC-CHO** exhibited green fluorescence with λ_{max} at 505 nm, while the protected probes exhibited fluorescence intensity at a slightly lower wavelength (λ_{max} = 455 nm) (Fig. S1d–f, ESI†). To gain a deeper insight into the optical properties of **DPIC-OS** and **DPIC-SS**, a preliminary solvent study was performed to assess their absorbance and emission behavior in various organic solvents (Table S1, ESI†). Of the organic solvents selected, both **DPIC-OS** and **DPIC-SS** probes exhibited better emission properties in DMSO with a broad peak at around 455 nm with quantum yields of 36% and 39%, respectively, using quinine sulfate as the standard, while in other solvents the probes exhibited lower quantum yields.[52] Mercury ion contamination is largely prevalent in aquatic bodies, par-

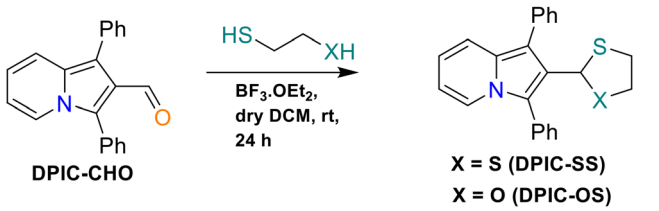

Scheme 1 General procedure for synthesizing the **DPIC-SS** and **DPIC-OS** probes.

ticularly sea water; therefore, pure aqueous media are ideal for the detection of Hg^{2+} ions. As **DPIC-OS** and **DPIC-SS** are insoluble in water, an organic–aqueous mixed medium was initially chosen for the detection of mercury. Therefore, stock solutions of the probes (1 mM) in DMSO and ACN were prepared separately and utilized for mercury detection. Separately, 10 μL of **DPIC-OS** and **DPIC-SS** (1 mM) stock solution was added to water and mercury ions were then gradually added, and respective fluorescence spectra recorded (Fig. 1a). The organic–aqueous system exhibited poor fluorescence intensity, with minimal changes upon the addition of mercury ions (Fig. 1b). Presumably, as chemodosimeters undergo a chemical reaction to generate a fluorometric change, the hydrophobic **DPIC-OS** and **DPIC-SS** require an organic environment to react with mercury ions. The organic–aqueous mixed media simply could not provide sufficient solvation of the probes for the reaction to occur.[43,53] Thus, we were encouraged to use micellar media for chemodosimetric detection of Hg^{2+} ions using **DPIC-OS** and **DPIC-SS**. Three surfactants with contrasting head groups, *viz*. cetyltrimethylammonium bromide (CTAB) (cationic), sodium dodecyl benzene sulfonate (SDBS) (anionic), and Triton X-100 (neutral) were chosen as the additives for the sensing systems. First, the UV-Vis spectra of **DPIC-OS** and **DPIC-SS** were recorded in a micellar medium, revealing minimal spectral changes (Fig. S2a, ESI†). As expected, the subsequent addition of CTAB and Triton X-100 (above the CMC) led to a significant increase in the fluorescence signals of **DPIC-OS** and **DPIC-SS**, with the fluorescence intensity in the surfactant solutions being comparable to that in organic solvents, indicating that the probes are in a relatively hydrophobic environment (Fig. S2b and c, ESI†). Interestingly, in the case of SDBS, the probes exhibited minimal changes in fluorescence output. Although the probes exhibited a relatively higher quantum yield in Triton X-100 than that in other surfactants, it was noticed that the probes demonstrated better responses to mercury ions with greater Stokes shifts when CTAB was chosen as the micelle-forming agent (Fig. 1b and Table S2, ESI†). A study with varying concentrations of CTAB, below the CMC, at the CMC, and above the CMC, was carried out to understand the effect of the micellar microenvironment on fluorescence output. As expected, the CTAB concentration at and above the CMC facilitated similar or better fluorescence enhancement compared to that of organic solvents, while below the CMC, no enhancement was noted (Fig. S3, ESI†). Before proceeding further, a time-dependent response study of both **DPIC-OS** (10 μM) and **DPIC-SS** (10 μM) with mercury ions (25 μM) in CTAB was conducted. It was observed that the maximum fluorescence output was achieved within just 2 min for **DPIC-OS** but took 15 min for **DPIC-SS** (Fig. S4, ESI†). The seemingly faster FL output of the **DPIC-OS** probe can be attributed to the labile hemiacetal bond formed after the cleavage of the C–S bond by Hg^{2+} ions. In order to establish pH stability, the emissive properties of **DPIC-CHO**, **DPIC-OS** and **DPIC-SS** were evaluated over a broad range of pH values (3–11). The pH study revealed that all three compounds showed no changes in their fluorescence output at neutral pH, with the best results being obtained at a pH value of 7.4, indicating their potential to be used under physiological conditions (Fig. S5, ESI†). Presumably, due to the acid-sensitive nature of thioacetals, **DPIC-OS** and **DPIC-SS** showed higher fluorescence intensity under acidic conditions, indicating their cleavage to generate the parent aldehyde group. As **DPIC-OS** exhibited better fluorescence output in a shorter time, this combination was chosen for further analytical studies.

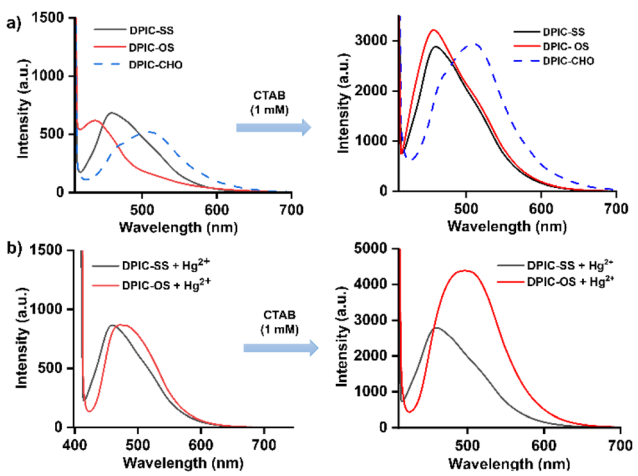

Fig. 1 (a) Fluorescence signal intensity of **DPIC-SS**, **DPIC-OS**, and **DPIC-CHO** (10 μM) before and after surfactant (CTAB) addition (λ_{ex} = 400 nm). (b) The change in fluorescence intensity of **DPIC-SS** and **DPIC-OS** in the presence of mercury before and after surfactant addition (1 mM CTAB; λ_{ex} = 400 nm).

2.3 Detection of Hg^{2+} ions

Initially, an organic aqueous system containing 10 μL of **DPIC-OS** (1 mM in DMSO) in 5% DMSO-HEPES buffer was utilized for the detection of mercury ions. The fluorescence output of **DPIC-OS** exhibited a gradual increase with a slight bathochromic shift from 445 nm to 494 nm upon the gradual addition of mercury ions (Fig. 2a). The shift in peak is presumably due to the generation of **DPIC-CHO** formed after the cleavage of the oxathiolane moiety. The relative fluorescence intensity exhibited a gradual increase with saturation after the addition of 80 μM Hg^{2+} ions upon incubation for 30 min. The high concentration of mercury ions required and longer response time are possibly due to phase separation in the microenvironment, the preference of Hg^{2+} ions to remain in the aqueous phase, and also the low dispersibility of the **DPIC-OS** probe in aqueous solutions (Fig. 2b). A linear relationship between the relative fluorescence output and the concentration of mercury ions with a good regression coefficient (R^2 = 0.9185) was observed within the lower concentration range (0–5 μM). Following the linear plot, a mediocre detection limit of 0.55 μM (109 ppb) was calculated using the formula $3\sigma/k$, where σ is the standard deviation and k is the slope of the calibration curve. Next, the sensing analysis was carried out in the micellar media containing 1 mM CTAB.

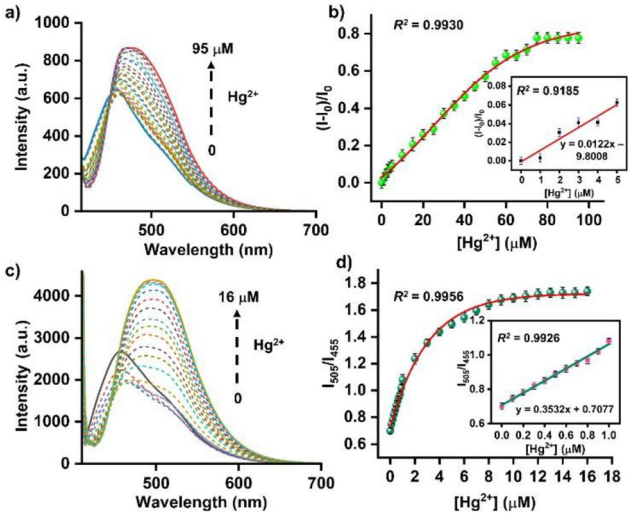

Fig. 2 (a) Fluorescence signals of **DPIC-OS** (10 μM in 5% DMSO-HEPES buffer) upon gradual addition of Hg^{2+} (0–95 μM) (λ_{ex} = 400 nm; λ_{em} = 455 nm, 495 nm). (b) The relative fluorescence output of **DPIC-OS** (10 μM in 5% DMSO-HEPES buffer) upon gradual addition of Hg^{2+} ions [inset: linear correlation between relative fluorescence intensity and concentration of Hg^{2+} ions within the lower range]. (c) Fluorescence signals of **DPIC-OS** (10 μM in micellar media using 1.0 mM CTAB) upon gradual addition of Hg^{2+} ions (0–16 μM) (λ_{ex} = 400 nm; λ_{em} = 455 nm, 505 nm). (d) Plot of the ratio of fluorescence intensities against Hg^{2+} concentrations (0–16 μM) [inset: ratio of the fluorometric responses of **DPIC-OS** to lower concentrations of mercury ions].

Upon addition of mercury ions to **DPIC-OS**, a bathochromic shift from 455 nm to 505 nm, similar to that of the aqueous–organic mixture, was noted (Fig. 2c). However, the increase in fluorescence output after the addition of increasing concentrations of mercury ions was greatly enhanced with almost a four-fold increase while the response time was significantly decreased to 2 min. The enhancement in fluorescence response was proportional to the concentration of Hg^{2+} ions added and reached saturation upon the addition of about one equiv. of Hg^{2+} ions. The FL output exhibited a linear response within the lower concentration range of 0.1–1.0 μM Hg^{2+}, with a high regression coefficient of 0.9926 (Fig. 2d). Based on these data, the limit of detection (LOD) was determined to be 16.2 nM (3.2 ppb) using the same formula as above. This ensures the advantage of using a micellar microenvironment for analyte detection in the aqueous phase.

As both **DPIC-OS** and **DPIC-CHO** exhibited a strong absorption band in the UV–vis spectrum at 290 nm and 400 nm, investigations were conducted to monitor absorption changes in the presence and absence of Hg^{2+} ions. Upon incubation with Hg^{2+} ions (0–17 μM), a gradual increase in the absorption peak at around 400 nm was noted, with saturation again occurring at 12 μM Hg^{2+} ions (Fig. S6a, ESI†). The corresponding increase revealed a linear trend from 1 to 10 μM, and from the graph, the detection limit was found to be 94 ppb or 0.47 μM (Fig. S6b, ESI†). Similarly, the absorption spectrum of **DPIC-SS** was recorded with additions of Hg^{2+} ions (0–22 μM), which also showed a linear response over the 1–10 μM range (Fig. S5c and d, ESI†). Thus, both **DPIC-OS** and **DPIC-SS** can work as fluorometric and colorimetric dual-output probes in chemodosimeters for mercury ions.

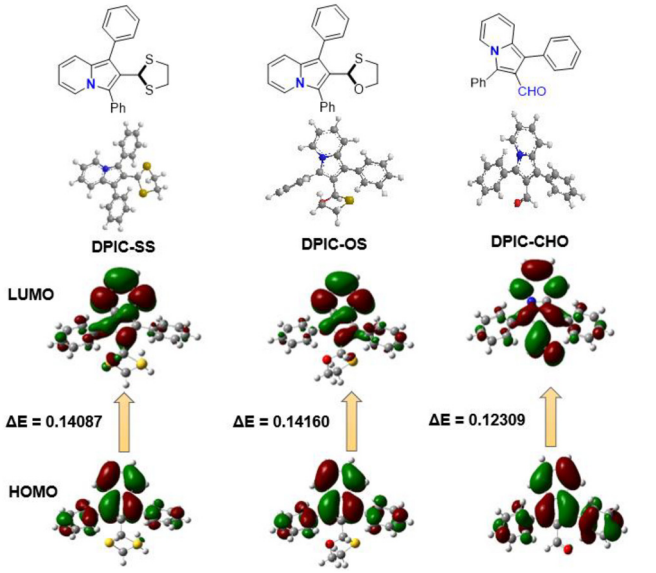

Fig. 3 Optimized structures, visualized electron distribution and energy levels of the ground state HOMO and LUMO of **DPIC-SS**, **DPIC-OS** and **DPIC-CHO**.

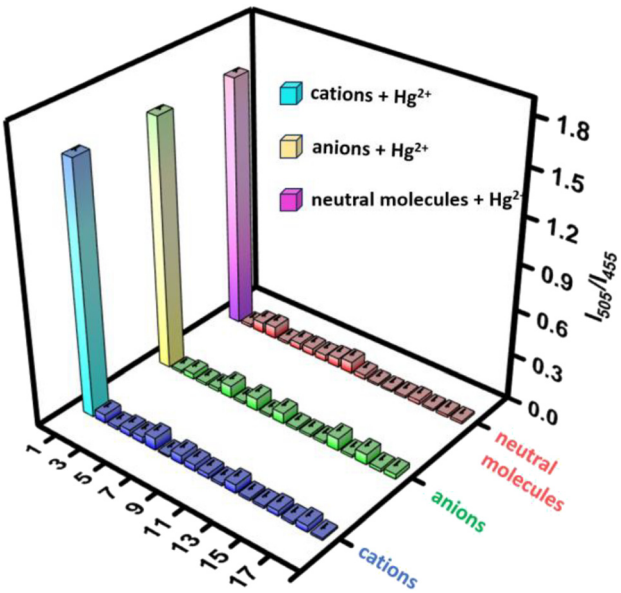

Fig. 4 Selective fluorescence output of the **DPIC-OS** probe against cations (1. all cations + Hg^{2+}, 2. Ca^{2+}, 3. Na^{+}, 4. Mg^{2+}, 5. K^{+}, 6. Ag^{+}, 7. Al^{3+}, 8. Cd^{2+}, 9. Co^{2+}, 10. Cu^{2+}, 11. Cr^{3+}, 12. Fe^{3+}, 13. Mn^{2+},14. Ni^{2+}, 15. Pb^{2+} 16. Zn^{2+}, 17. Ba^{2+} 18. Sn^{2+}), anions (1. all anions + Hg^{2+}, 2. F^{-}, 3. Cl^{-}, 4. Br^{-}, 5. I^{-}, 6. SCN^{-}, 7. CO_3^{2-}, 8. NO_2^{-}, 9. NO_3^{-}, 10. AcO^{-}, 11. SO_4^{2-}, 12. $S_2O_3^{2-}$, 13. $S_2O_4^{2-}$, 14. CN^{-}, 15. N_3^{-}, 16. PO_4^{3-}, 17. HS^{-}, 18. S^{2-}), and small molecules (1. all small molecules + Hg^{2+}, 2. Ala, 3. Arg, 4. Gly, 5. Leu, 6. Lys, 7. glucose, 8. urea, 9. H_2O_2, 10. NH_2NH_2, 11. Phe, 12. Pro, 13. Spm, 14. Spd, 15. Mel, 16. His, 17. Tet, 18. Cip).

2.4 DFT studies

In order to gain better insights into the observed optical properties of the probes, DFT studies were conducted.[54] Both **DPIC-OS** and **DPIC-SS** exhibited similar results in DFT analysis with the electron population spread across the entire molecular structure with higher density on the indolizine moiety (Fig. 3). However, in **DPIC-CHO**, a shift was noticed, with the electron density delocalized in the aldehyde group. Presumably, due to the delocalizing effect of the oxygen atom, **DPIC-CHO** exhibited a lower energy gap than **DPIC-OS** and **DPIC-SS**, which indicates that the emission maxima for **DPIC-CHO** occur at a relatively higher wavelength, as experimentally observed.

2.5 Selectivity of DPIC-OS towards Hg^{2+}

Following the successful detection of mercury ions (Hg^{2+}), the next essential step was to assess and mitigate any interference from other species in the detection process. A comprehensive study was performed to identify potential competitors to Hg^{2+}, including different anions, metal ions, and neutral molecules (Fig. 4). The system demonstrated excellent selectivity for Hg^{2+} against other species, including cations such as Na^{+}, Mg^{2+}, Al^{3+}, Ag^{+}, and Pb^{2+}, anions including Cl^{-}, Br^{-}, and I^{-}, and small molecules such as glucose, amino acids, urea, H_2O_2, *etc.*, indicating the feasibility of **DPIC-OS** as a selective fluorometric sensor for mercury ions. The high specificity is attributed to the strong thiophilic affinity of Hg^{2+}, which selectively cleaves the oxathiolane moiety in **DPIC-OS**, triggering the release of **DPIC-CHO** and causing the subsequent fluorescence shift. These results confirm that **DPIC-OS** functions as a highly selective chemodosimeter probe for Hg^{2+} detection without cross-reactivity from other potential interfering agents (Fig. 4).

2.6 Sensing mechanism

The sensing mechanism capitalizes on the thiophilicity of Hg^{2+} ions. In micellar media, the addition of mercury ions induces a reaction with **DPIC-OS**, resulting in the cleavage of the C–S bond. This results in the formation of a hemiacetal, which quickly breaks down to generate **DPIC-CHO**, and show bluish-green fluorescence (Fig. 5). Micelles are not rigid entities and remain in dynamic equilibrium with their monomeric form.[55] An organic probe prefers to stay inside the hydrophobic interior of the micelle but may have access to the water sink. Presumably, **DPIC-OS** hops from one micellar core to another *via* the water sink in a dynamic transition and interacts with mercury ions close to the CTAB-derived micelles near its head group or in the water sink to facilitate the cleavage of the oxathiolane group. Once **DPIC-CHO** is formed, it enters into

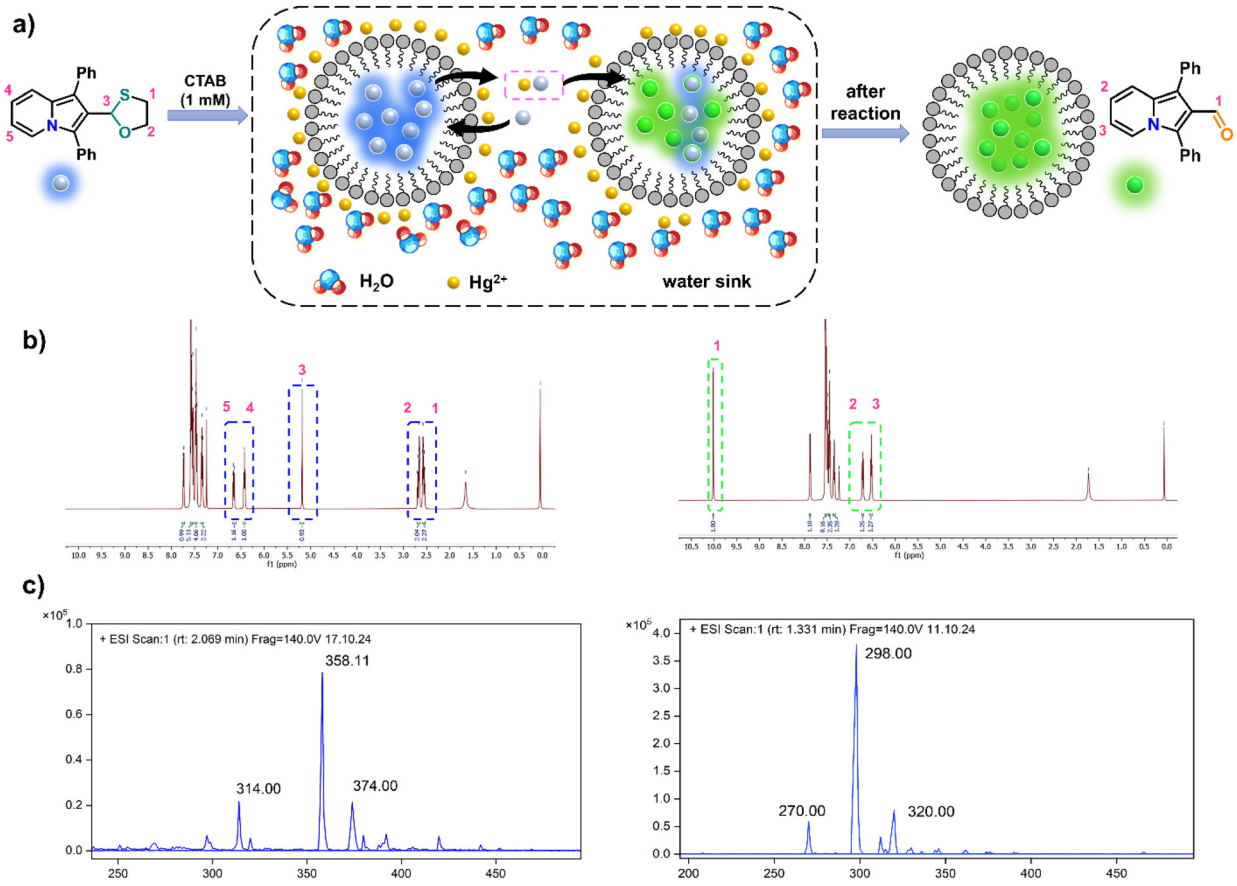

Fig. 5 (a) The sensing mechanism of the detection of mercury ions by **DPIC-OS** in micellar media. The changes in (b) ^{1}H NMR and (c) LC-MS spectra of **DPIC-OS** before and after the addition of mercury ions.

the micellar microenvironment and exhibits enhanced fluorescence (Fig. 5a). In order to confirm the sensing mechanism, a bulk-scale reaction was conducted by interacting **DPIC-OS** with 2 equiv. of mercury ions in a micellar medium at room temperature, keeping the reaction conditions similar to the sensing conditions. After 30 min of stirring, the product was isolated with ethyl acetate and subjected to NMR spectroscopy. The ^{1}H NMR spectrum matched well with the original NMR spectrum of **DPIC-CHO** (Fig. 5b). Also, in the mass spectral analysis of a sample extracted from the sensing solution, the spectrum showed a peak at *m*/*z* 298 obtained from LC-MS, which corresponds to the $[M + H]^+$ of **DPIC-CHO** (Fig. 5c). The above results firmly established the proposed mechanism of detection of mercury ions during this chemodosimetric approach *via* the cleavage of the oxathiolane moiety in micellar media.

2.7 Real-sample analysis

Numerous studies have shown mercury contamination in natural water sources, highlighting the critical need for its detection and removal. To demonstrate the indolizine-based probe's real-world applications, water samples from ponds, rivers, the sea, tap water, lakes, and rain were collected and spiked with known concentrations of Hg^{2+} ions. The spiked samples were incubated with the probe, and their fluorescence was measured. Each test was performed in triplicate, with a relative standard deviation (RSD) of 3–4%, indicating the reproducibility of the results. The %recovery for all real samples using **DPIC-OS** was above 95% (Table 1), indicating the efficient functioning of the sensing assay in detecting mercury ions in real water samples, while the %recovery for all real samples using **DPIC-SS** was above 88% (Table S3, ESI†), indicating that **DPIC-OS** is superior to **DPIC-SS** when functioning as a fluorescent probe in sensing assays for detecting mercury ions in real water samples.

2.8 Comparative study

Finally, a comparative analysis of **DPIC-OS** against other conventional and water-soluble fluorescent probes for detection of mercury ions was conducted, focusing on key differences in sensitivity, selectivity, photostability, and practical applicability (Tables S4 and S5, ESI†). Compared to other probes, **DPIC-OS** demonstrates superior selectivity and quicker response times owing to its oxathiolane group and exhibited an LOD at the ppb level. Notably, several existing probes use significant amounts of organic solvents in aqueous media, which is sometimes as high as 50%, and even if they show low LOD values, they often require longer incubation periods. In contrast, in the case of **DPIC-OS**, the detection is carried out in a micellar medium ensuring that the sensing system is biocompatible.

Table 1 Analysis of real water samples using the **DPIC-OS** probe

S. no.	Sample	Spiked concentration (μM)	Obtained concentration (μM)	%Recovery	%RSD (n = 3)
1	Rain water	0.116	0.114	98	3.2
2	Tap water	0.064	0.061	95	3.5
3	Pond water	0.064	0.061	95	2.7
4	Sea water	0.062	0.059	95	3.1
5	River water	0.046	0.044	96	2.9

3. Conclusions

In this study, we developed two efficient fluorescent probes, **DPIC-OS** and **DPIC-SS**, derived from a less-explored indolizine scaffold, for highly selective and sensitive turn-on sensing of mercury ions (Hg^{2+}) exhibiting a distinct blue-to-green fluorescence transition in aqueous micellar media. The probes were obtained by protecting 1,3-diphenylindolizine-2-carbaldehyde (**DPIC-CHO**) with mercury-recognizable 1,3-dithiolane and 1,3-oxathiolane moieties. Although these hydrophobic probes demonstrated intense fluorescence in organic solvents, their fluorescence was significantly reduced in mixed aqueous–organic solvents due to the poor solubility of the probe, and they were found to be less effective for mercury detection. The addition of CTAB to provide a micellar microenvironment aided their solubility and this proved effective as the fluorescence of **DPIC-CHO**, **DPIC-OS**, and **DPIC-SS** was considerably enhanced. Presumably, the micelles can encapsulate the probe and provide a hydrophobic environment improving the fluorescence emission and sensing efficiency. **DPIC-OS** showed better sensing ability than **DPIC-SS**. In CTAB-derived micellar media, **DPIC-OS** could detect mercury ions through the release of fluorescent **DPIC-CHO**, which exhibits bluish-green emission at 505 nm. The probe demonstrated excellent selectivity towards mercury ions in the presence of various competing cations (*e.g.*, Na^+, Mg^{2+}, Al^{3+}, Ag^+), anions (*e.g.*, Cl^-, Br^-, I^-), and neutral molecules (*e.g.*, amino acids, glucose, urea). This exceptional specificity is attributed to the chemodosimetric sensing mechanism, which leverages the strong thiophilicity of mercury to trigger the deprotection of **DPIC-OS**. The probe demonstrated considerably low limits of detection of 3.2 ppb (16.2 nM) and 94 ppb (0.47 μM) in fluorometry and colorimetry, respectively. The successful application of **DPIC-OS** in real-sample analysis, including spiked water, with excellent recovery rates, underscores its potential for practical environmental monitoring and public health applications.

Author contributions

A. A. P.: investigation, analysis, validation, and writing – original draft. A. T.: validation, visualization, and writing – original draft and editing. S. S.: synthesis of the probe. M. B.: project administration, supervision, writing – original draft, and review & editing. Amrita Chatterjee: conceptualization, supervision, project administration, and writing – review & editing.

Data availability

The data supporting this article have been included as part of the ESI.†

Conflicts of interest

There are no conflicts of interest to declare.

Acknowledgements

A. C. acknowledges the financial support from DBT BUILDER-BITS Pilani, KK Birla Goa Campus Interdisciplinary Life Science program (No. BT/INF/22/SP42543/2021) and UGC-DAE(CSR) (CRS/2021-22/02/502). A. A. P., A. T., and S. S. acknowledge BITS Pilani, KK Birla Goa campus for its fellowship. The authors acknowledge the Central Sophisticated Instrumentation Facility (CSIF), BITS, Pilani, KK Birla Goa Campus, for NMR and ESI-MS analyses. DST-FIST (No. SR/FST/CSI-232-2011) is acknowledged for providing computational facilities to the Department of Chemistry.

References

1 R. Dietz, C. Sonne, N. Basu, B. Braune, T. O'Hara, R. J. Letcher, T. Scheuhammer, M. Andersen, C. Andreasen, D. Andriashek, G. Asmund, A. Aubail, H. Baagøe, E. W. Born, H. M. Chan, A. E. Derocher, P. Grandjean, K. Knott, M. Kirkegaard, A. Krey, N. Lunn, F. Messier, M. Obbard, M. T. Olsen, S. Ostertag, E. Peacock, A. Renzoni, F. F. Rigét, J. U. Skaare, G. Stern, I. Stirling, M. Taylor, Ø. Wiig, S. Wilson and J. Aars, What are the toxicological effects of mercury in Arctic biota?, *Sci. Total Environ.*, 2013, **433**, 775–790.

2 C. T. Driscoll, R. P. Mason, H. M. Chan, D. J. Jacob and N. Pirrone, Mercury as a global pollutant: Sources, pathways, and effects, *Environ. Sci. Technol.*, 2013, **10**, 4967–4983.

3 N. Basu, A. Bastiansz, J. G. Dórea, M. Fujimura, M. Horvat, E. Shroff and I. Zastenskaya, Our evolved understanding of the human health risks of mercury, *Ambio*, 2023, **5**, 877–896.

4 M. Rallo, M. A. Lopez-Anton, M. L. Contreras and M. M. Maroto-Valer, Mercury policy and regulations for coal-fired power plants, *Environ. Sci. Pollut. Res.*, 2012, **19**, 1084–1096.

5 L. J. Esdaile and J. M. Chalker, The mercury problem in artisanal and small-scale gold mining, *Chem. – Eur. J.*, 2018, **24**, 6905–6916.

6 H. Agarwalla, R. N. Senapati and T. B. Das, Mercury emissions and partitioning from Indian coal-fired power plants, *J. Environ. Sci.*, 2021, **100**, 28–33.

7 V. Kumar, M. Umesh, M. K. Shanmugam, P. Chakraborty, L. Duhan, S. N. Gummadi, R. Pasrija, I. Jayaraj and L. K. D. Huligowda, A retrospection on mercury contamination, bioaccumulation, and toxicity in diverse environments: current insights and future prospects, *Sustainability*, 2023, **15**, 13292.

8 M. M. Storelli, R. Giacominelli-Stuffler, A. Storelli and G. O. Marcotrigiano, Accumulation of mercury, cadmium, lead, and arsenic in swordfish and bluefin tuna from the Mediterranean Sea: A comparative study, *Mar. Pollut. Bull.*, 2005, **50**, 1004–1007.

9 P. Pereira, J. Raimundo, O. Araújo, J. Canário, A. Almeida and M. Pacheco, Fish eyes and brain as primary targets for mercury accumulation—A new insight on environmental risk assessment, *Sci. Total Environ.*, 2014, **494–495**, 290–298.

10 S. J. Cobbina, Y. Chen, Z. Zhou, X. Wu, W. Feng, W. Wang, M. Guanghua, X. Hai, Z. Zhang, X. Wu and L. Yang, Low concentration toxic metal mixture interactions: Effects on essential and non-essential metals in brain, liver, and kidneys of mice on sub-chronic exposure, *Chemosphere*, 2015, **132**, 79–86.

11 K. M. Rice Jr., E. M. Walker, M. Wu, C. Gillette and E. R. Blough, Environmental mercury and its toxic effects, *J. Prev. Med. Public Health*, 2014, **2**, 74–83.

12 L. T. Budnik and L. Casteleyn, Mercury pollution in modern times and its socio-medical consequences, *Sci. Total Environ.*, 2019, **654**, 720–734.

13 G. Genchi, M. S. Sinicropi, A. Carocci, G. Lauria and A. Catalano, Mercury exposure and heart diseases, *Int. J. Environ. Res. Public Health*, 2017, **14**, 74.

14 A. Qureshi, Mercury in the environment around industrially impacted locations in India: A mini-review, *Bull. Environ. Contam. Toxicol.*, 2022, **6**, 937–942.

15 E. V. Ramasamy, K. K. Jayasooryan, M. S. Chandran and M. Mohan, Total and methyl mercury in the water, sediment, and fishes of Vembanad, a tropical backwater system in India, *Environ. Monit. Assess.*, 2017, **189**, 1–19.

16 P. Chakraborty, S. Jayachandran, J. Lekshmy, P. Padalkar, L. Sitlhou, K. Chennuri, S. Shetye, A. Sardar and R. Khandeparker, Seawater intrusion and resuspension of surface sediment control mercury (Hg^{2+}) distribution and its bioavailability in water column of a monsoonal estuarine system, *Sci. Total Environ.*, 2019, **660**, 1441–1448.

17 A. Jaswal, S. Swami and A. Saini, Mercury (Hg^{2+}) sensing using Coumarin-derived fluorescent chemo-sensors: An Intuitive Development from 2015 to 2023, *J. Fluoresc.*, 2024, 1–33.

18 Safe Drinking Water Act, United States Environmental Protection Agency (USEPA) 1991, **https://www.epa.gov/sdwa/drinking-water-regulations-and-contaminants**.

19 J. K. Fawell, U. Lund and B. Mintz, Guidelines for drinking-water quality, in *Health criteria and other supporting information*, World Health Organization, Geneva, 2nd edn, 1996, vol. 2.

20 M. K. Rofouei, A. Sabouri, A. Ahmadalinezhad and H. Ferdowsi, Solid phase extraction of ultra traces mercury (II) using octadecyl silica membrane disks modified by 1,3-bis(2-ethoxyphenyl)triazene (EPT) ligand and determination by cold vapor atomic absorption spectrometry, *J. Hazard. Mater.*, 2011, **192**, 1358–1363.

21 M. E. Foulkes, S. L. Roux and R. Muñoz-Olivas, Cold vapour atomic fluorescence spectrometry and gas chromatography-pyrolysis-atomic fluorescence spectrometry for

routine determination of total and organometallic mercury in food samples, *Analyst*, 2002, **127**, 1108–1114.
22 J. S. dos Santos, M. de la Guárdia, A. Pastor and M. L. P. dos Santos, Determination of organic and inorganic mercury species in water and sediment samples by HPLC on-line coupled with ICP-MS, *Talanta*, 2009, **80**, 207–211.
23 D. Martín-Yerga, M. B. Gonzalez-García and A. Costa-García, Electrochemical determination of mercury: A review, *Talanta*, 2013, **116**, 1091–1104.
24 C. Gao and X. J. Huang, Voltammetric determination of mercury(II), *TrAC, Trends Anal. Chem.*, 2013, **51**, 1–12.
25 G. Chen, Z. Guo, G. Zeng and L. Tang, Fluorescent and colorimetric sensors for environmental mercury detection, *Analyst*, 2015, **140**, 5400–5443.
26 H. N. Kim, W. X. Ren, J. S. Kim and J. Yoon, Fluorescent and colorimetric sensors for detection of lead, cadmium, and mercury ions, *Chem. Soc. Rev.*, 2012, **8**, 3210–3244.
27 J. Ding, H. Li, C. Wang, J. Yang, Y. Xie, Q. Peng, Q. Li and Z. Li, "Turn-On" fluorescent probe for mercury(II): High selectivity and sensitivity and new design approach by the adjustment of the π-bridge, *ACS Appl. Mater. Interfaces*, 2015, **7**, 11369–11376.
28 Y. Gao, N. Yi, Z. Ou, Z. Li, T. Ma, H. Jia and Y. Li, Thioacetal modified phenanthroimidazole as fluorescence probe for rapid and sensitive detection of Hg^{2+} in aqueous solution assisted by surfactant, *Sens. Actuators, B*, 2018, **267**, 136–144.
29 G. Zhang, D. Zhang, S. Yin, X. Yang, Z. Shuai and D. Zhu, 1,3-Dithiole-2-thione derivatives featuring an anthracene unit: New selective chemodosimeters for Hg(II) ion, *Chem. Commun.*, 2005, **2005**, 2161–2163.
30 E. Bozkurt and H. I. Gul, A novel pyrazoline-based fluorometric "turn-off" sensing for Hg^{2+}, *Sens. Actuators, B*, 2018, **255**, 814–825.
31 E. Bozkurt and H. I. Gul, Selective fluorometric "Turn-off" sensing for Hg2+ with pyrazoline compound and its application in real water sample analysis, *Inorg. Chim. Acta*, 2020, **502**, 119288.
32 M. Hong, S. Lu, F. Lv and D. Xu, A novel facilely prepared rhodamine-based Hg^{2+} fluorescent probe with three thiourea receptors, *Dyes Pigm.*, 2016, **127**, 94–99.
33 B. Gu, L. Huang, W. Su, X. Duan, H. Li and S. Yao, A benzothiazole-based fluorescent probe for distinguishing and bioimaging of Hg^{2+} and Cu^{2+}, *Anal. Chim. Acta*, 2017, **954**, 97–104.
34 S. Madhu, S. Josimuddin and M. Ravikanth, 3,5-Bis (dithioacetal) meso-aryl BODIPYs: Selective chemodosimeters for Hg(II) ions, *New J. Chem.*, 2014, **38**, 3770–3776.
35 A. S. Rao, D. Kim, T. Wang, K. H. Kim, S. Hwang and K. H. Ahn, Reaction-based two-photon probes for mercury ions: Fluorescence imaging with dual optical windows, *Org. Lett.*, 2012, **14**, 2598–2601.
36 X. Cheng, Q. Li, J. Qin and Z. Li, A new approach to design ratiometric fluorescent probe for mercury(II) based on the Hg^{2+}-promoted deprotection of thioacetals, *ACS Appl. Mater. Interfaces*, 2010, **2**, 1066–1072.
37 Z. Ruan, Y. Shan, Y. Gong, C. Wang, F. Ye, Y. Qiu, Z. Liang and Z. Li, Novel AIE-active ratiometric fluorescent probes for mercury(II) based on the Hg^{2+}-promoted deprotection of thioketal, and good mechanochromic properties, *J. Mater. Chem. C*, 2018, **6**, 773–780.
38 J. R. Lakowicz, *Principles of fluorescence spectroscopy*, Plenum, New York, Springer, New York, NY, 1993.
39 G. E. Dobretsov, T. I. Syrejschikova and N. V. Smolina, On mechanisms of fluorescence quenching by water, *Biophysics*, 2014, **59**, 183–188.
40 J. Maillard, K. Klehs, C. Rumble, E. Vauthey, M. Heilemann and A. Fürstenberg, Universal quenching of common fluorescent probes by water and alcohols, *Chem. Sci.*, 2021, **12**, 1352–1362.
41 P. Mahato, S. Saha, P. Das, H. Agarwalla and A. Das, An overview of the recent developments on Hg^{2+} recognition, *RSC Adv.*, 2014, **4**, 36140–36174.
42 K. Muthu Vengaian, C. D. Britto, K. Sekar, G. Sivaraman and S. Singaravadivel, Phenothiazine-diaminomalenonitrile based colorimetric and fluorescence "turn-off-on" sensing of Hg^{2+} and S^{2-}, *Sens. Actuators, B*, 2016, **235**, 232–240.
43 D. Patra and C. Barakat, Unique role of ionic liquid [bmin][BF_4] during curcumin–surfactant association and micellization of cationic, anionic and non-ionic surfactant solutions, *Spectrochim. Acta, Part A*, 2011, **79**, 1823–1828.
44 Y. D. Fernandez, A. P. Gramatges, V. Amendola, F. Foti, C. Mangano, P. Pallavicini and S. Patroni, Using micelles for a new approach to fluorescent sensors for metal cations, *Chem. Commun.*, 2004, **2004**, 1650–1651.
45 Y. Zhao and Z. Zhong, Detection of Hg^{2+} in aqueous solutions with a foldamer-based fluorescent sensor modulated by surfactant micelles, *Org. Lett.*, 2006, **21**, 4715–4717.
46 R. Wu, M. Tian, C. Shu, C. Zhou and W. Guan, Determination of the critical micelle concentration of surfactants using fluorescence strategies, *Soft Matter*, 2022, **18**, 8920–8930.
47 S. D. Hiremath, K. K. Maiti, N. N. Ghosh, M. Banerjee and A. Chatterjee, Reduced graphene oxide–thioguanine composites for the selective detection of inorganic and organic mercury in aqueous media, *ACS Appl. Nano Mater.*, 2020, **3**, 3071–3079.
48 A. Thakuri, A. A. Bhosle, S. D. Hiremath, M. Banerjee and A. Chatterjee, A carbon dots-MnO_2 nanosheet-based turn-on pseudochemodosimeter as low-cost probe for selective detection of hazardous mercury ion contaminations in water, *J. Hazard. Mater.*, 2024, **469**, 133998.
49 A. Airine, R. Tigoianu, R. Danac, C. M. Al Matarneh and D. L. Isac, Steady state and time resolved fluorescence studies of new indolizine derivatives with phenanthroline skeleton, *J. Lumin.*, 2018, **199**, 6–12.
50 X. Liu, H. Fu, Q. Hu and H. Cao, Recent advances on the construction of functionalized indolizine and imidazo [1,2-a]pyridine derivatives, *Chem. Rec.*, 2024, **24**, e202400135.

51 Y. C. Yuan, T. Z. Liu and B. X. Zhao, Metal-free catalyzed synthesis of fluorescent indolizine derivatives, *J. Org. Chem.*, 2021, **86**, 12737–12744.
52 A. M. Brouwer, Standards for photoluminescence quantum yield measurements in solution (IUPAC Technical Report), *Pure Appl. Chem.*, 2011, **83**, 2213–2228.
53 R. Germani, P. Anastasio, M. Chiodini, T. Del Giacco, Tiecco and M. L. Belpassi, Fluorescent signal transduction in a self-assembled Hg^{2+} chemosensor tuned by various interactions in micellar aqueous environment, *J. Photochem. Photobiol., A*, 2020, **389**, 112276.
54 R. R. Parr and R. G. Yang, *Density functional theory of atoms and molecules*, Oxford University Press, New York, 1989, Search PubMed.
55 B. H. Lipshutz, When does organic chemistry follow nature's lead and "make the switch"?, *J. Org. Chem.*, 2017, **82**, 2806–2816.